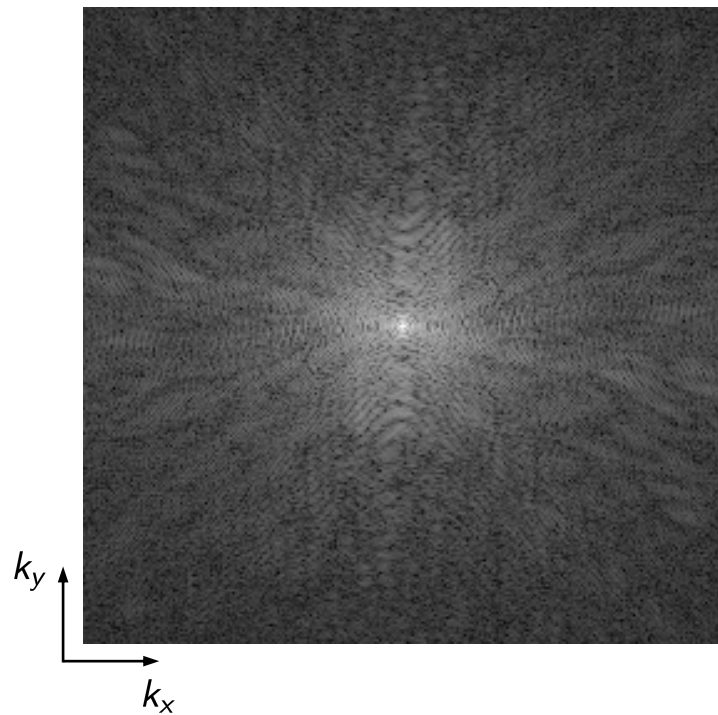


# Computational MRI

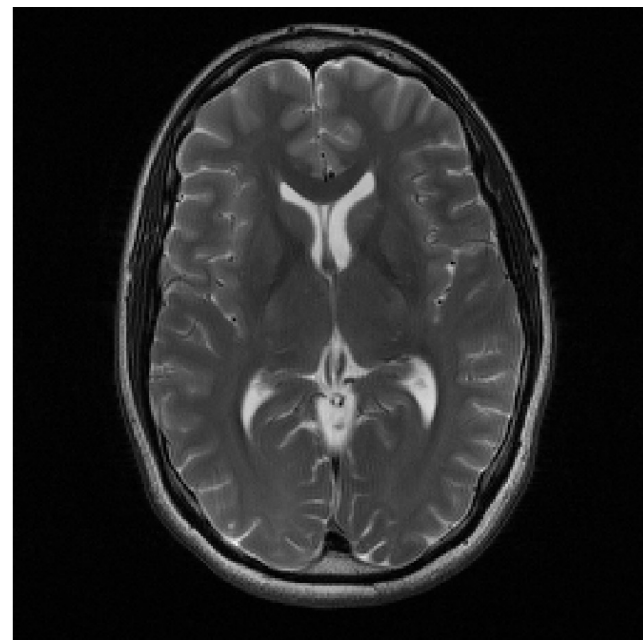
## Reconstruction of Non-Cartesian MRI Data

# K-space

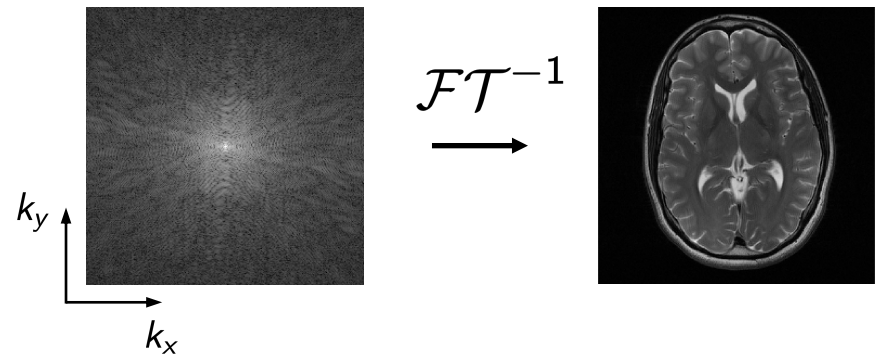
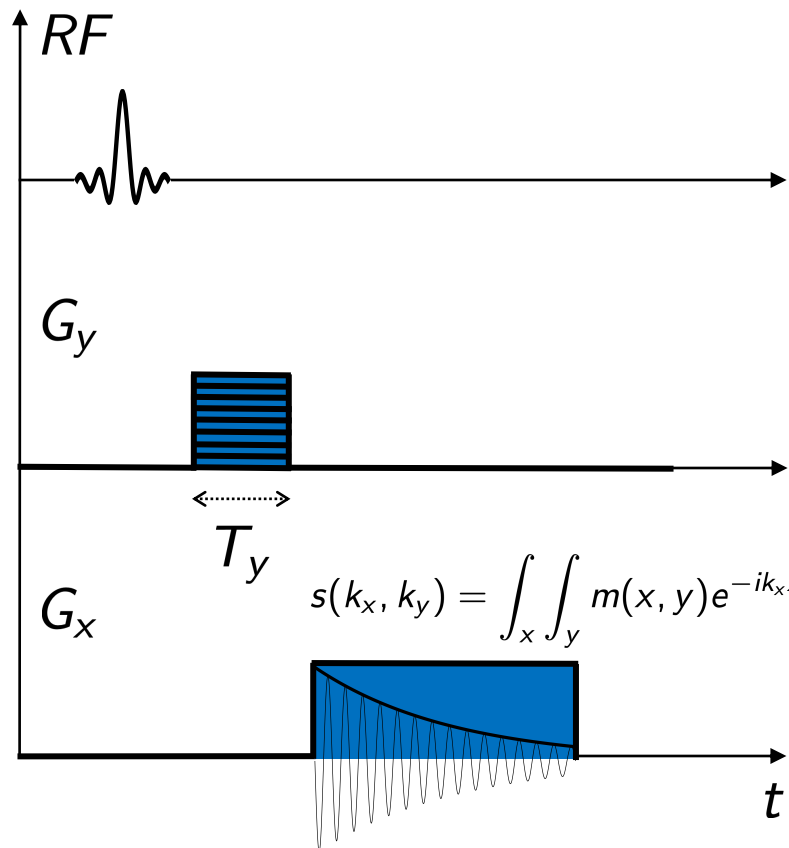
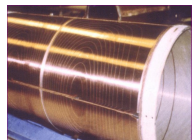


$$\mathcal{FT}^{-1}$$

An arrow pointing from the K-space image to the reconstructed image, indicating the inverse Fourier transform process.



# Gradient fields and K-space



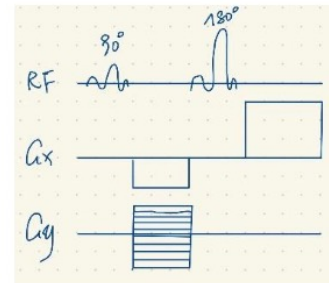
$$s(k_x, k_y) = \int_x \int_y m(x, y) e^{-ik_x x} e^{-ik_y y} dx dy$$

$$\phi(x, t) = \gamma x \int_0^t G_x d\tau \equiv k_x x$$

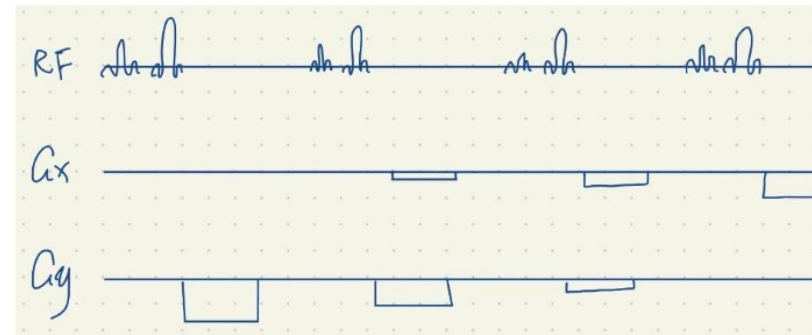
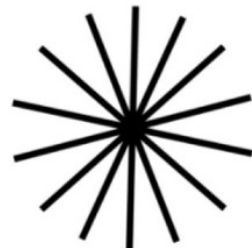
$$\phi(y, G_y) = \gamma y \int_0^{T_y} G_y d\tau \equiv k_y y$$

# Gradient fields and K-space

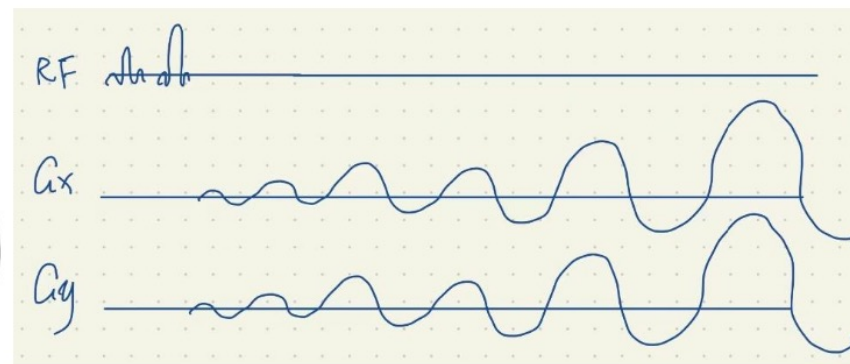
Cartesian



Radial

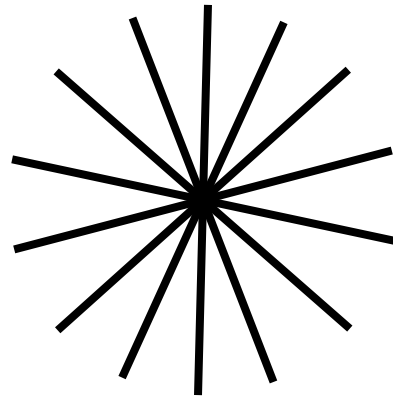


Spiral

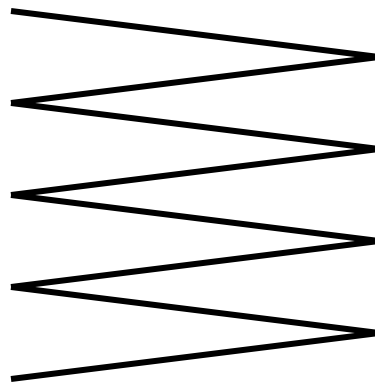


# Non-Cartesian MRI

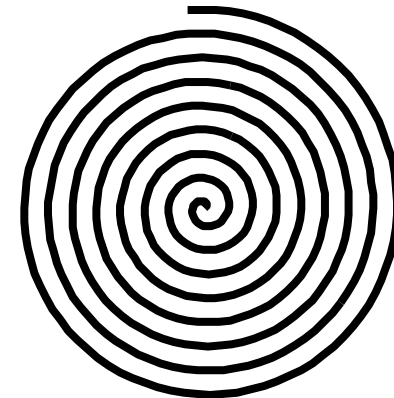
Radial



EPI



Spiral



- Pros: fast, motion-robust, self-navigation
- Cons: Susceptible to hardware imperfections (off-resonance, gradient linearity, eddy currents)
- Cons: Numerically more challenging reconstruction

# Reconstruction of non-Cartesian MRI data

- Direct FFT does not work
- Radial MRI
  - Backprojection reconstruction, like in CT
- In general
  - DFT: Compute the inverse Fourier transform according to the trajectory (slow)
  - Gridding: resample the non-Cartesian MRI data into a Cartesian grid and apply inverse FFT (fast)

# Filtered backprojection reconstruction (CT)

# Original MRI experiment

## Image Formation by Induced Local Interactions: Examples Employing Nuclear Magnetic Resonance

An image of an object may be defined as a graphical representation of the spatial distribution of one or more of its properties. Image formation usually requires that the object interact with a matter or radiation field characterized by a wavelength comparable to or smaller than the smallest features to be distinguished, so that the region of interaction may be restricted and a resolved image generated.

This limitation on the wavelength of the field may be removed, and a new class of image generated, by taking advantage of induced local interactions. In the presence of a second field that restricts the interaction of the object with the first field to a limited region, the resolution becomes independent of wavelength, and is instead a function of the ratio of the normal width of the interaction to the shift produced by a gradient in the second field. Because the interaction may be regarded as a coupling of the two fields by the object, I propose that image formation by this technique be known as zeugmatography, from the Greek ζευγμα, "that which is used for joining".

The nature of the technique may be clarified by describing two simple examples. Nuclear magnetic resonance (NMR) zeugmatography was performed with 60 MHz (5 m) radiation and a static magnetic field gradient corresponding, for proton resonance, to about  $700 \text{ Hz cm}^{-1}$ . The test object consisted of two 1 mm inside diameter thin-walled glass capillaries of  $\text{H}_2\text{O}$  attached to the inside wall of a 4.2 mm inside diameter glass tube of  $\text{D}_2\text{O}$ . In the first experiment, both capillaries contained pure water. The proton resonance line width, in the absence of the transverse field gradient, was about 5 Hz.

Assuming uniform signal strength across the region within the transmitter-receiver coil, the signal in the presence of a field gradient represents a one-dimensional projection of the  $\text{H}_2\text{O}$  content of the object, integrated over planes perpendicular to the gradient direction, as a function of the gradient coordinate (Fig. 1). One method of constructing a two-dimensional projected image of the object, as represented by its  $\text{H}_2\text{O}$  content, is to combine several projections, obtained by rotating the object about an axis perpendicular to the gradient direction (or, as in Fig. 1, rotating the gradient about the object), using one of the available methods for reconstruction of objects from their projections<sup>1-5</sup>. Fig. 2 was generated by an algorithm, similar to that of Gordon and Herman<sup>6</sup>, applied to four projections, spaced as in Fig. 1, so as to construct a  $20 \times 20$  image matrix. The representation shown was produced by shading within contours interpolated between the matrix points, and clearly reveals the locations and dimensions of the two columns of  $\text{H}_2\text{O}$ . In the second experiment, one capillary contained pure  $\text{H}_2\text{O}$ , and the other contained a 0.19 mM solution of  $\text{MnSO}_4$  in  $\text{H}_2\text{O}$ . At low radio-frequency power (about 0.2 mogauss) the two capillaries gave nearly identical images in the

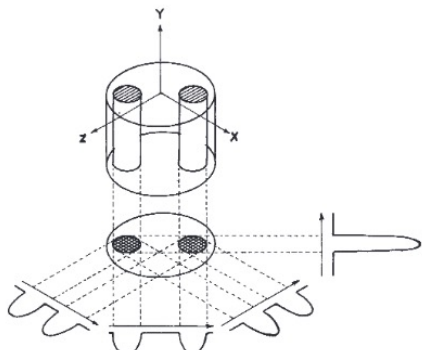


Fig. 1 Relationship between a three-dimensional object, its two-dimensional projection along the Y-axis, and four one-dimensional projections at  $45^\circ$  intervals in the XX-plane. The arrows indicate the gradient directions.



Fig. 2 Proton nuclear magnetic resonance zeugmatogram of the object described in the text, using four relative orientations of object and gradients as diagrammed in Fig. 1.

NATURE VOL. 242 MARCH 16 1973

NATURE VOL. 242 MARCH 16 1973

zeugmatogram (Fig. 3a). At a higher power level (about 1.6 mogauss), the pure water sample gave much more saturated signals than the sample whose spin-lattice relaxation time  $T_1$  had been shortened by the addition of the paramagnetic  $\text{Mn}^{2+}$  ions, and its zeugmatographic image vanished at the contour level used in Fig. 3b. The sample region with long  $T_1$  may be selectively emphasized (Fig. 3c) by constructing a difference zeugmatogram from those taken at different radio-frequency powers.

Applications of this technique to the study of various inhomogeneous objects, not necessarily restricted in size to those commonly studied by magnetic resonance spectroscopy, may be anticipated. The experiments outlined above demonstrate the ability of the technique to generate pictures of the distributions of stable isotopes, such as H and D, within an object. In the second experiment, relative intensities in an image were made to depend upon relative nuclear relaxation times. The variations in water contents and proton relaxation times among biological tissues should permit the generation, with field gradients large compared to internal magnetic inhomogeneities, of useful zeugmatographic images from the rather sharp water resonances of organisms, selectively picturing the various soft structures and tissues. A possible application of considerable interest at this time would be to the *in vivo* study of malignant tumours, which have been shown to give proton nuclear magnetic resonance signals with much longer water spin-lattice relaxation times than those in the corresponding normal tissues<sup>6</sup>.

The basic zeugmatographic principle may be employed in many different ways, using a scanning technique, as described above, or transient methods. Variations on the experiment, to be described later, permit the generation of two- or three-dimensional images displaying chemical compositions, diffusion coefficients and other properties of objects measurable by spectroscopic techniques. Although applications employing nuclear magnetic resonance in liquid or liquid-like systems are simple and attractive because of the ease with which field gradients large enough to shift the narrow resonances by many

line widths may be generated, NMR zeugmatography of solids, electron spin resonance zeugmatography, and analogous experiments in other regions of the spectrum should also be possible. Zeugmatographic techniques should find many useful applications in studies of the internal structures, states, and compositions of microscopic objects.

P. C. LAUTERBUR

Department of Chemistry,  
State University of New York at Stony Brook,  
Stony Brook, New York 11790

Received October 30, 1972; revised January 8, 1973.

- <sup>1</sup> Bracewell, R. N., and Riddle, A. C., *Astrophys. J.*, **150**, 427 (1967).
- <sup>2</sup> Vainshtein, B. K., *Soviet Physics-Crystallography*, **15**, 781 (1971).
- <sup>3</sup> Ramachandran, G. N., and Lakshminarayanan, A. V., *Proc. US Nat. Acad. Sci.*, **68**, 2236 (1971).
- <sup>4</sup> Gordon, R., and Herman, G. T., *Comm. Assoc. Comput. Mach.*, **14**, 759 (1971).
- <sup>5</sup> Klug, A., and Crowther, R. A., *Nature*, **238**, 435 (1972).
- <sup>6</sup> Weisman, I. D., Bennett, L. H., Maxwell, Sr., L. R., Woods, M. W., and Burk, D., *Science*, **178**, 1288 (1972).

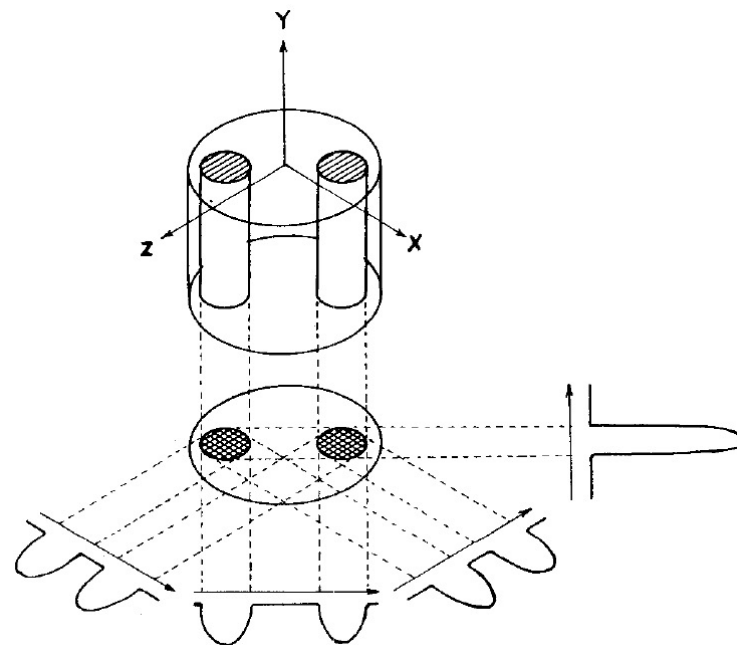


Fig. 3 Proton nuclear magnetic resonance zeugmatograms of an object containing regions with different relaxation times. a, Low power; b, high power; c, difference between a and b.

# Original MRI experiment

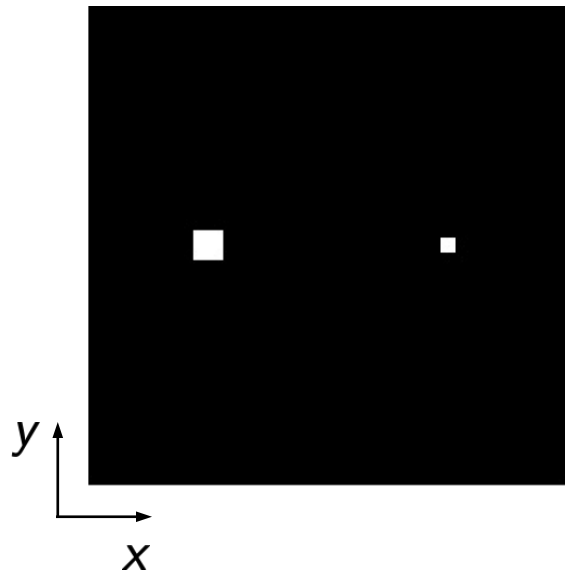
- Radial k-space sampling
- Filtered backprojection reconstruction

Image Formation by Induced Local Interactions: Examples Employing Nuclear Magnetic Resonance

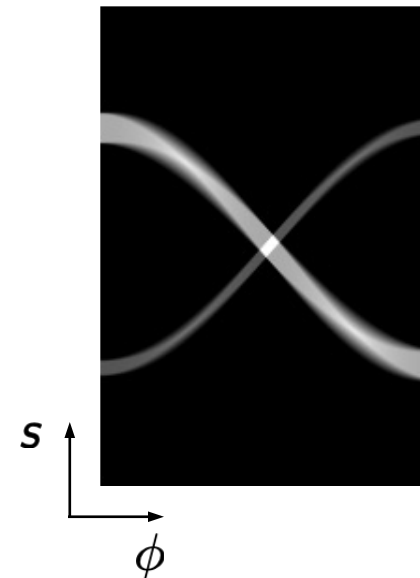
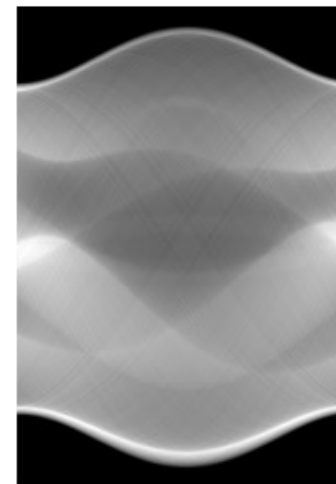


# Projections & the Radon transform

Image

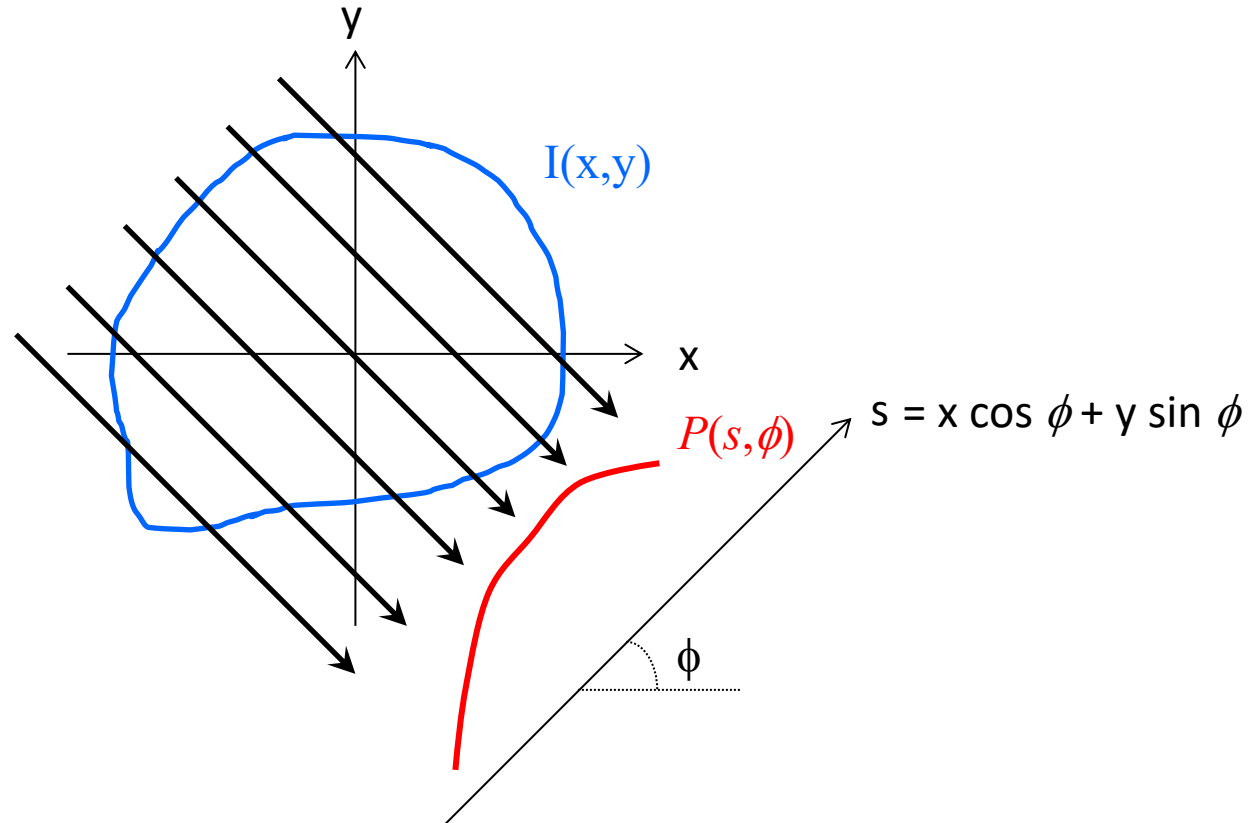


Radon space  
(sinogram)



# Projections & the Radon transform

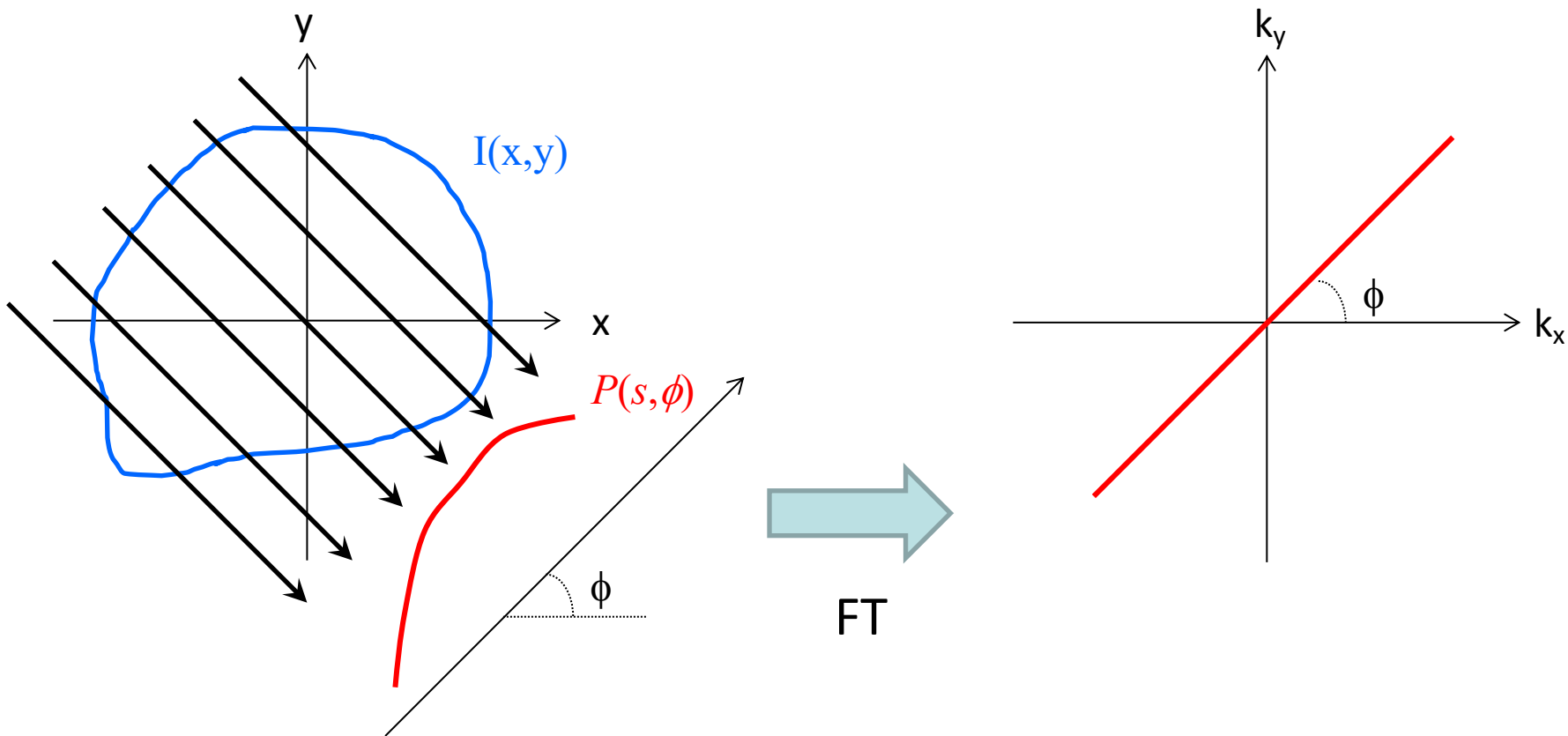
- Physical problem: parallel X-rays passing through an object



$$P(s, \phi) = \iint_{x, y} I(x, y) \delta(x \cos \phi + y \sin \phi - s) dx dy$$

# Fourier-slice theorem (a.k.a. central-slice theorem)

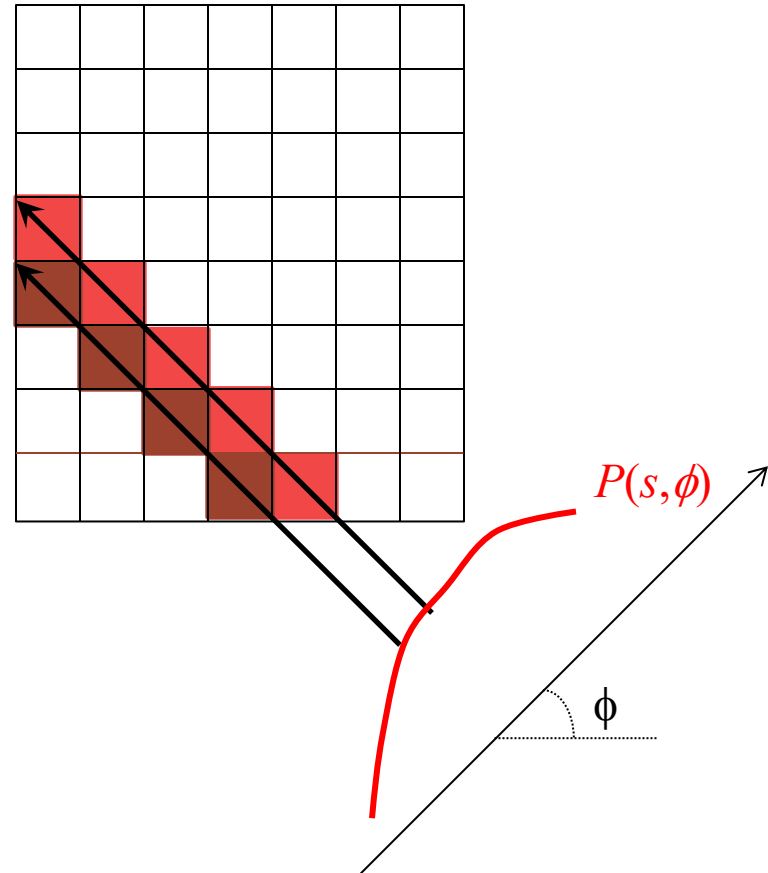
- The 1D Fourier transform of the projection at angle  $\phi$  is a radial line in k-space at angle  $\phi$



Fourier Slice Theorem: Bracewell (1956)

# Backprojection

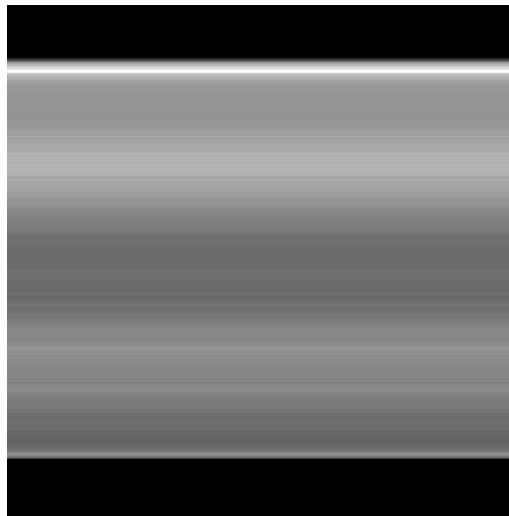
- Undo the projection
- Push ray through image matrix



# Backprojection

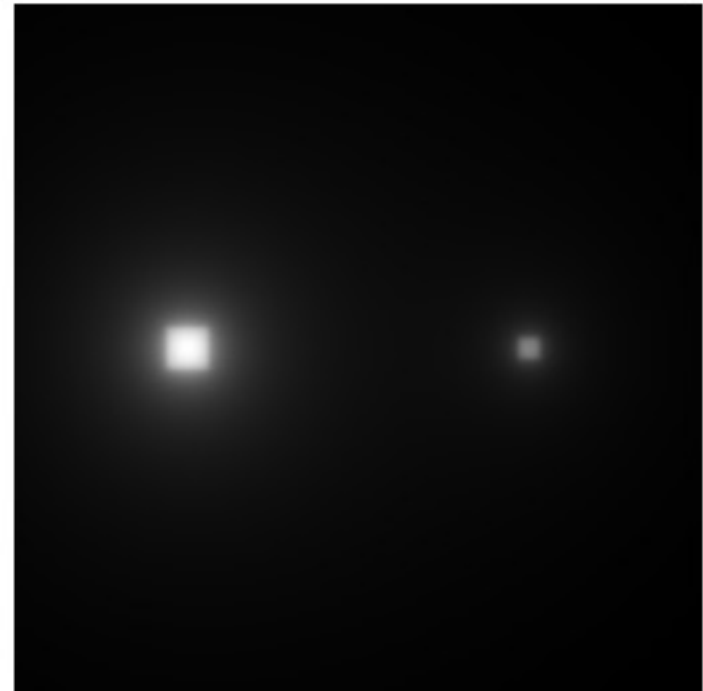
- Accumulate backprojections for all angles

$$b(x_i, y_i) = \sum_{m=1}^M P(x_i \cos \phi_m + y_i \sin \phi_m, \phi_m)$$



# Backprojection

- Straight backprojection leads to blurring

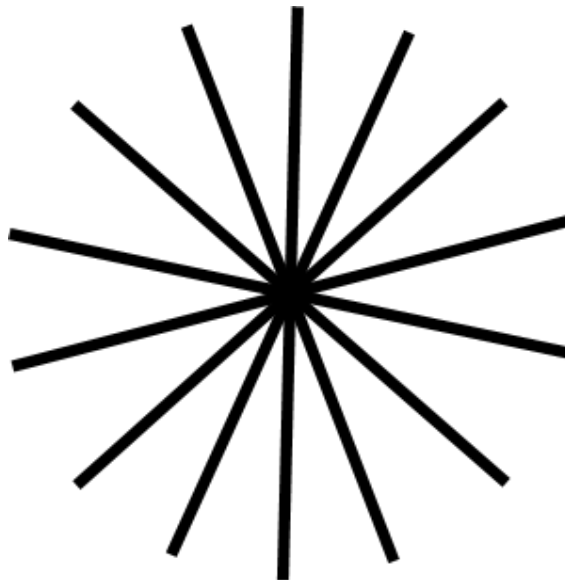


oversampling in the center,  
need to use filter

What is wrong?

# Backprojection

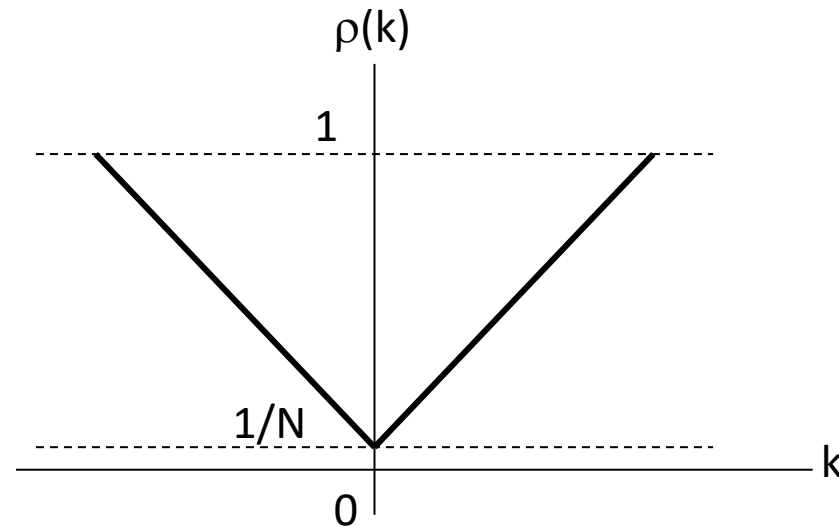
- Straight backprojection leads to blurring
  - Variable-density sampling in Fourier space (k-space)



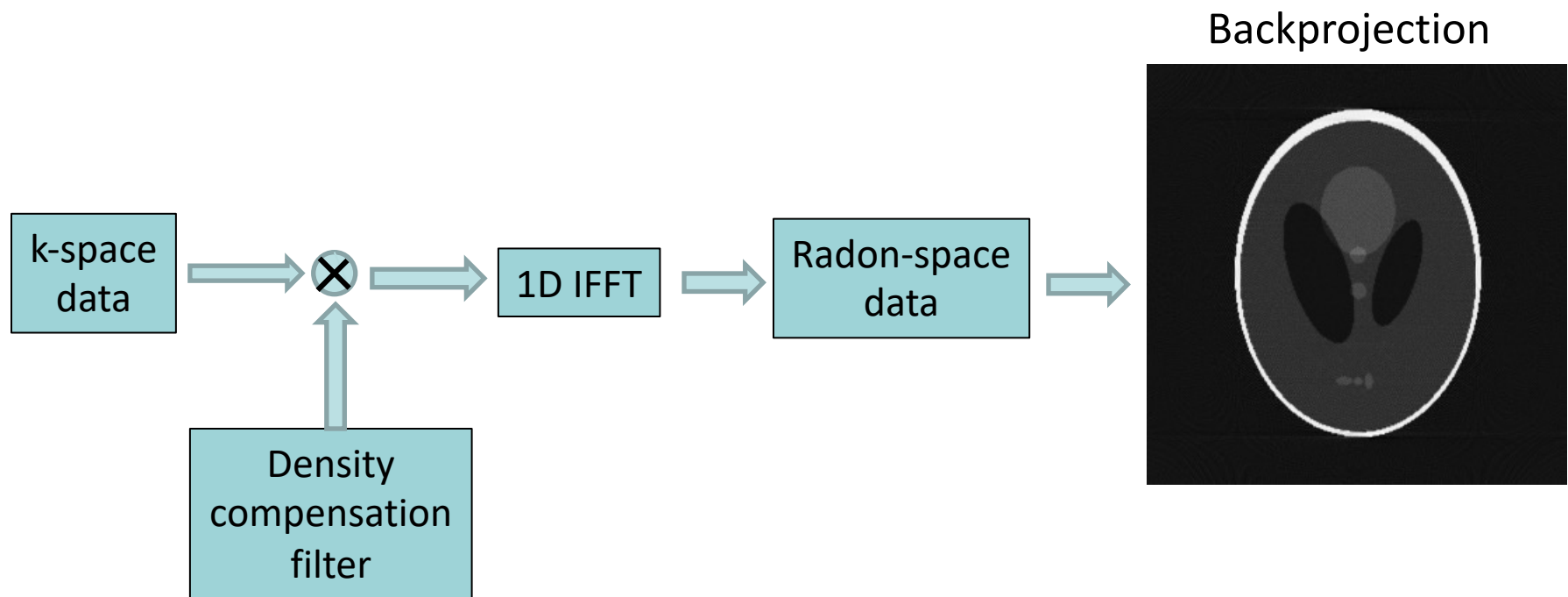
The center is  
acquired N times

# Filtered backprojection

- Density compensation in k-space
  - Ramp or rho filter



# Filtered backprojection algorithm

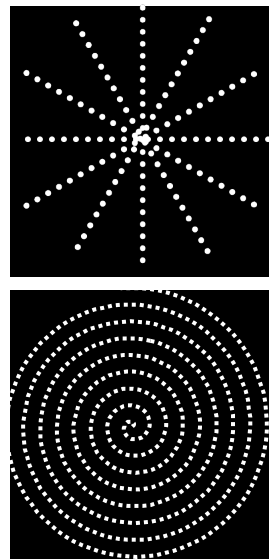


# Gridding reconstruction

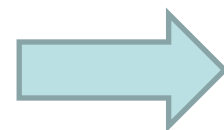
# Gridding

- Faster approach
- Convolution-based interpolation + FFT

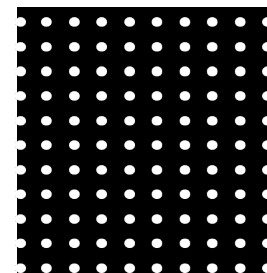
Non-Cartesian



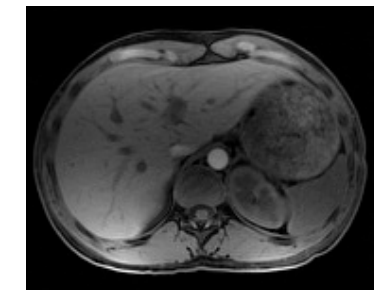
convolve  
&  
resample



Cartesian

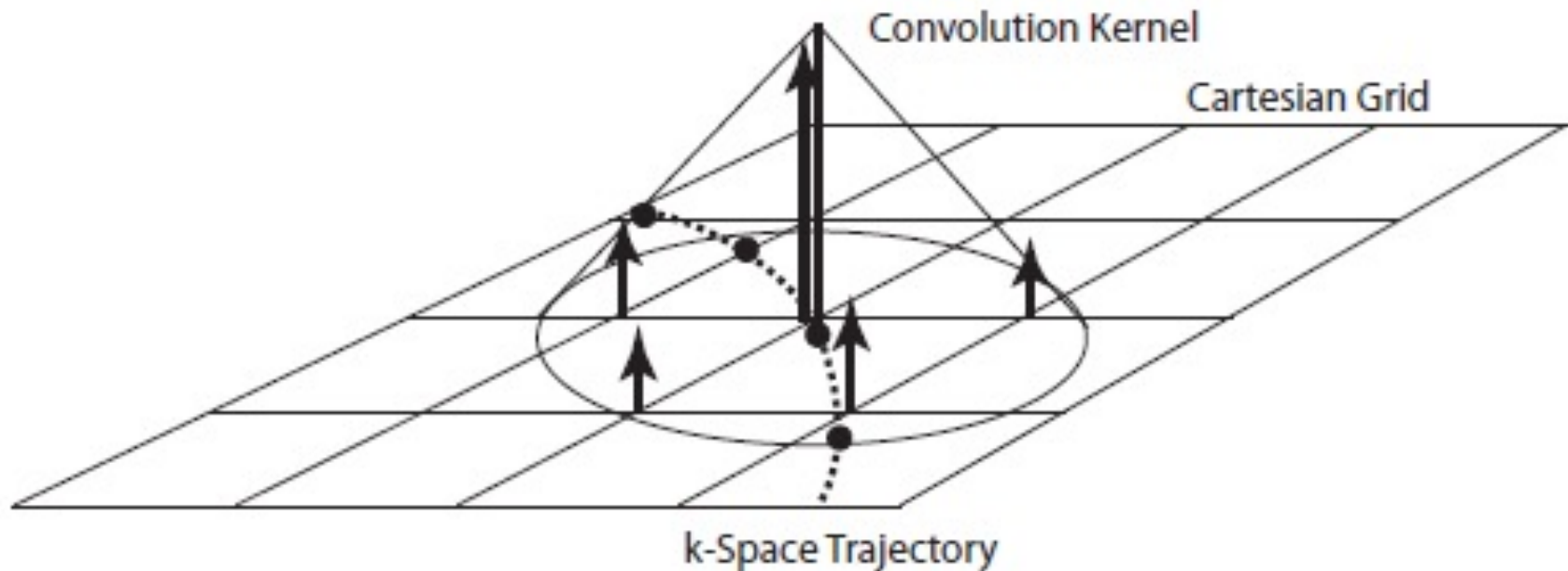


FFT



# Gridding

- Convolve with a k-space kernel
- Evaluate the convolution at the Cartesian grid



# Mathematical description of gridding

- Non-Cartesian sampling function:  $S(k_x, k_y) = \sum_i \delta(k_x - k_{x,i}, k_y - k_{y,i})$   
离散化sampling along the trajectory, 会导致PSF aliasing (unavoided)
- Sampled data:  $M(k_x, k_y)S(k_x, k_y)$
- Convolution with the gridding kernel and resampling on the Cartesian grid:

$$\hat{M}(k_x, k_y) = [(M(k_x, k_y)S(k_x, k_y)) * C(k_x, k_y)] \times III\left(\frac{k_x}{K_x}, \frac{k_y}{K_y}\right)$$

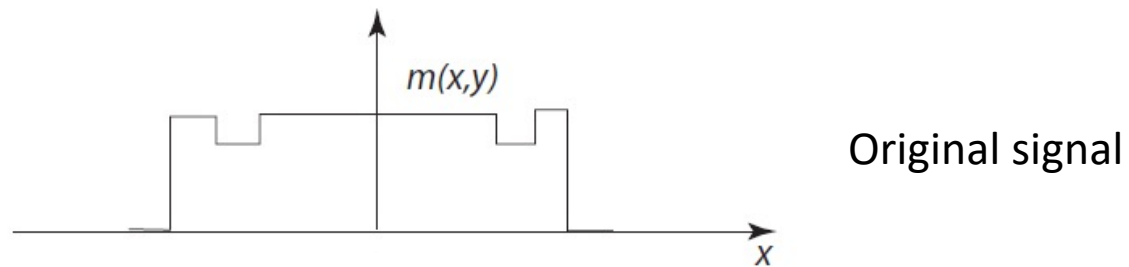
卷积gridding kernel 代表将kspace trajetoty  
上的samping point interpolate到Cartesian grid  
上

III: catesian grid,  
在全图推广

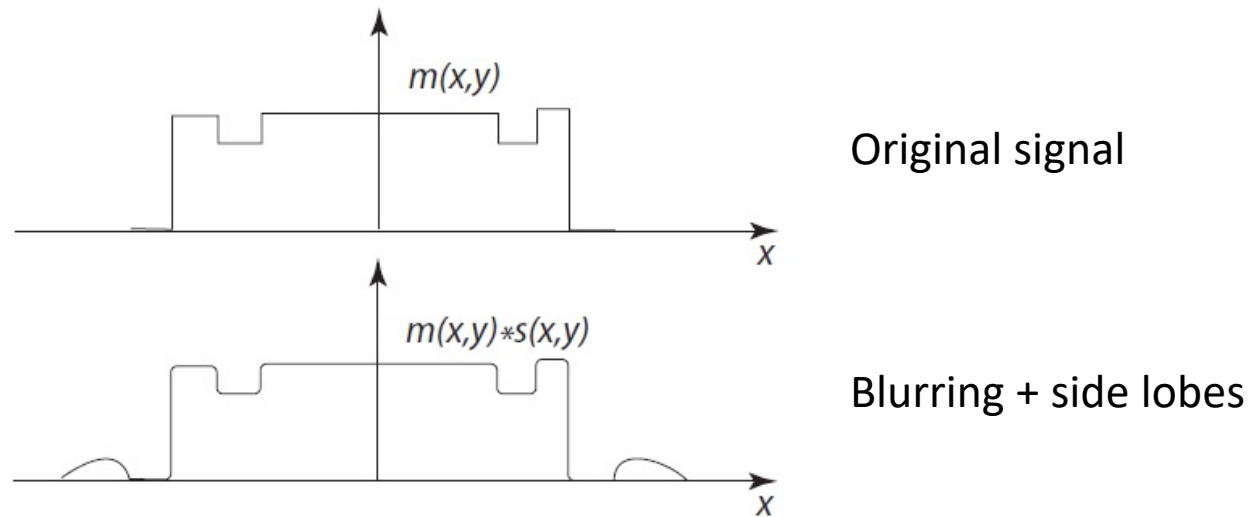
- After applying the inverse Fourier transform:

$$\hat{m}(x, y) = [(m(x, y) * s(x, y))c(x, y)] * III\left(\frac{x}{FOV_x}, \frac{y}{FOV_y}\right)$$

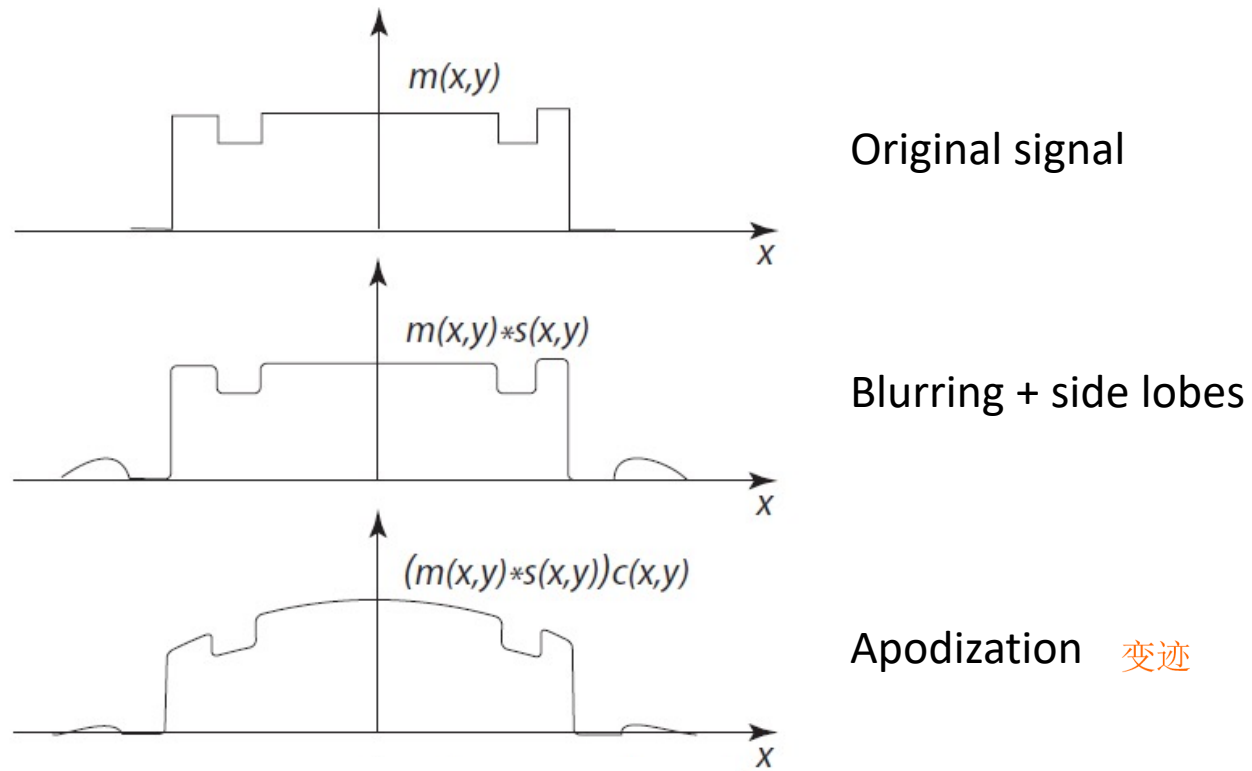
# Effect of gridding operations



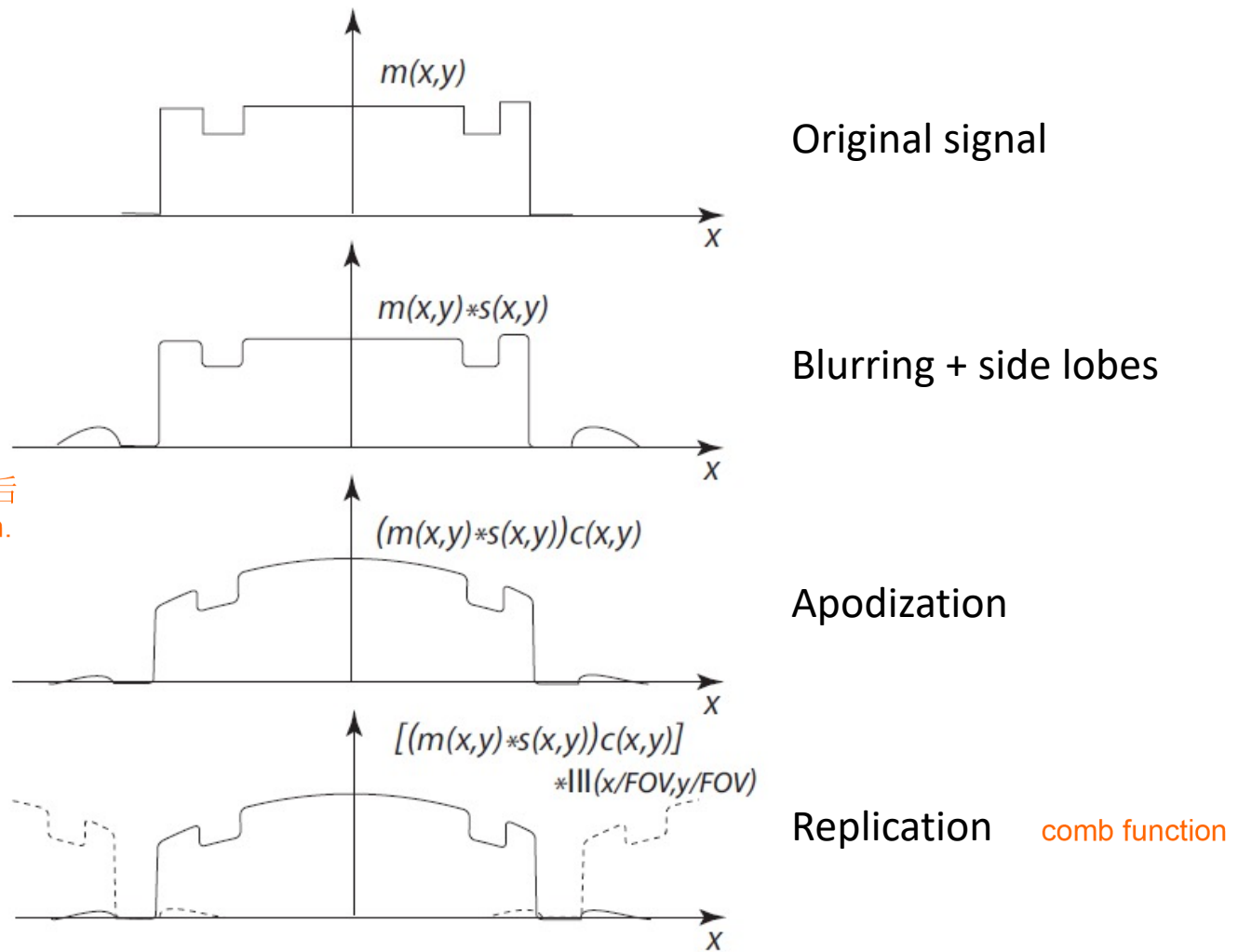
# Effect of gridding operations



# Effect of gridding operations



# Effect of gridding operations

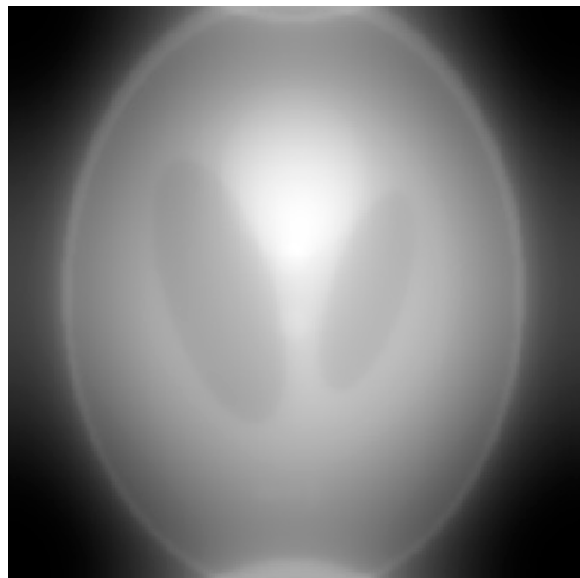


kernel- $c(x,y)$ 是triangle, FFT后是sinc func, 导致了apodization.  
最好的kernel是rectangular kernel但是它很computational expensive

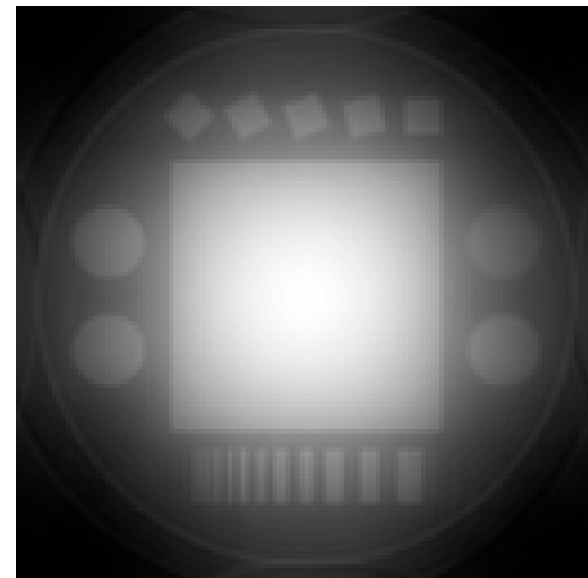
# Simple gridding

- 3-point triangular kernel

Radial k-space  
200x200 grid

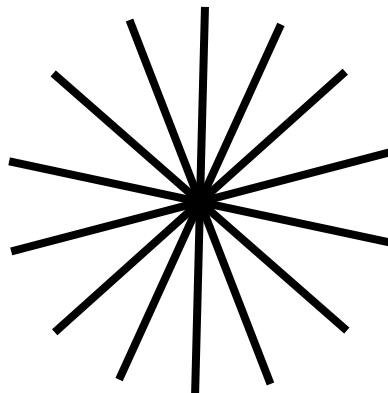


Spiral k-space  
128x128 grid



# Sampling density compensation

- Non-Cartesian trajectories sample k-space with variable density
  - Radial imaging: the central point is acquired N times



- Non-uniform k-space weighting

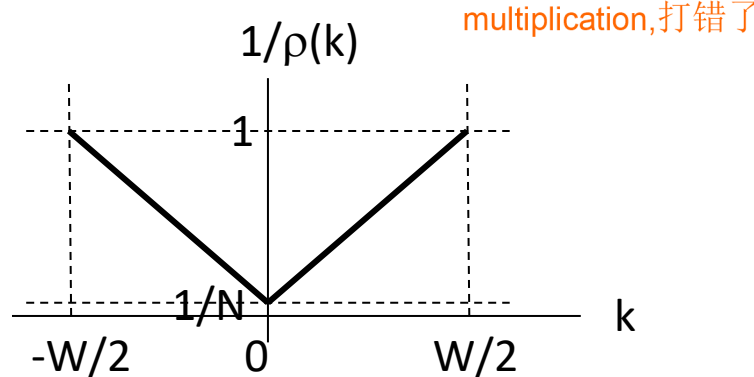
# Sampling density compensation

- Pre-compensation
  - Sampling density ( $\rho$ ) must be pre-computed

$$\hat{M}(k_x, k_y) = \left[ \left( \frac{M(k_x, k_y)}{\rho(k_x, k_y)} S(k_x, k_y) \right) * C(k_x, k_y) \right] * III\left( \frac{k_x}{\Delta k_x}, \frac{k_y}{\Delta k_y} \right)$$

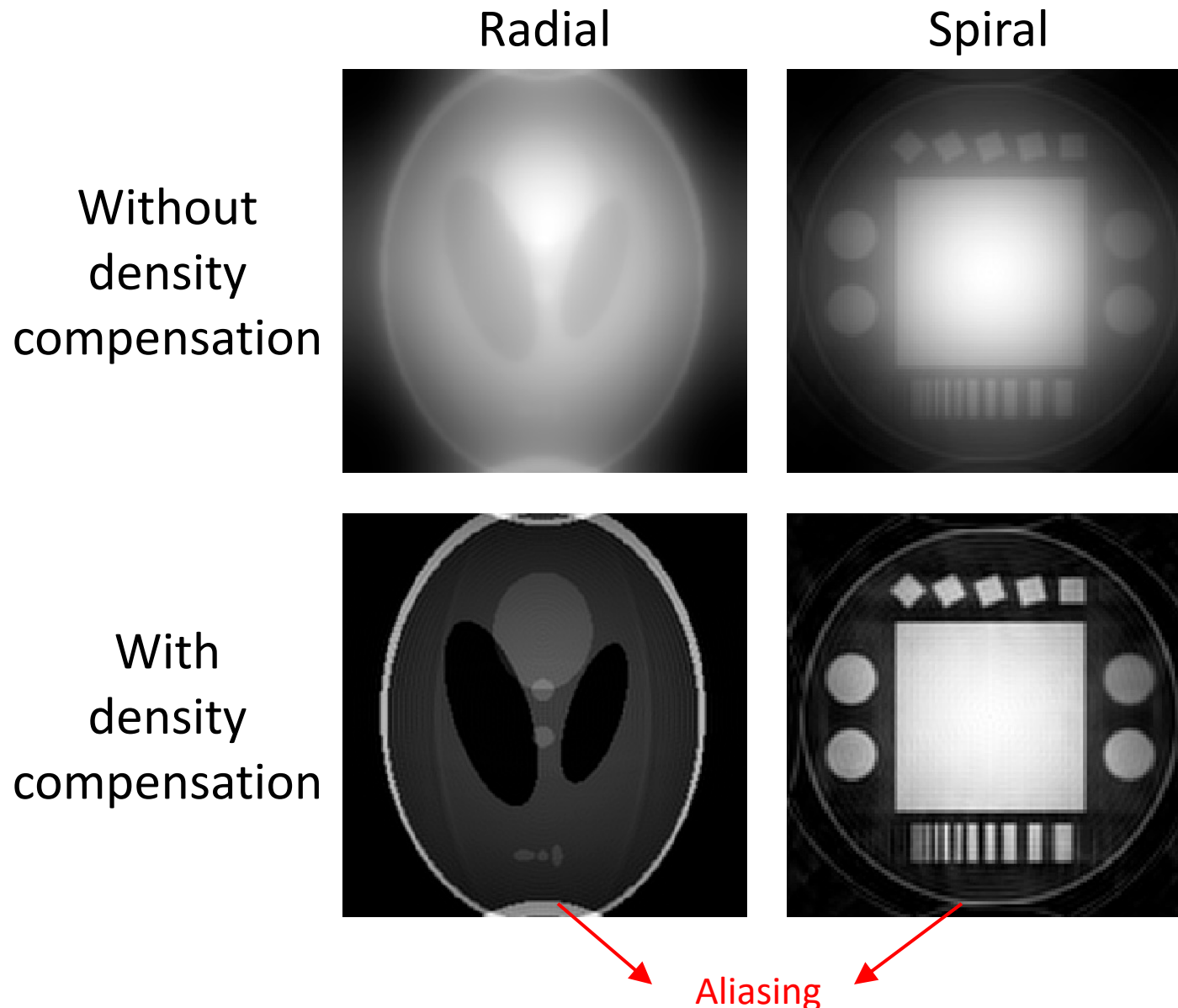
- Using geometry

For radial MRI:



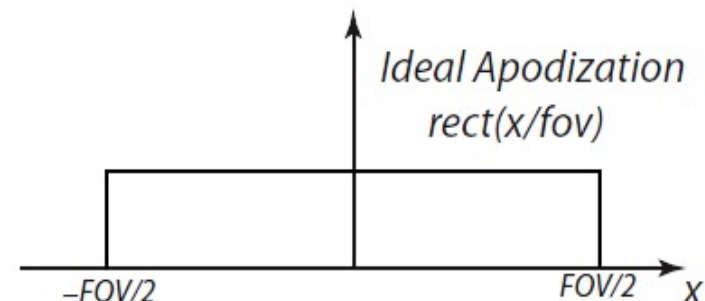
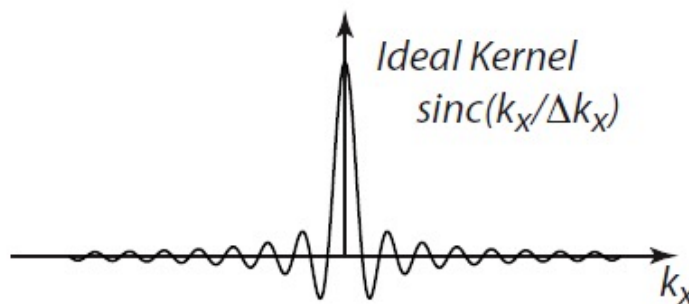
- Assign an area to each k-space sample (numerical method)
  - E.g. Voronoi diagram

# Sampling density compensation

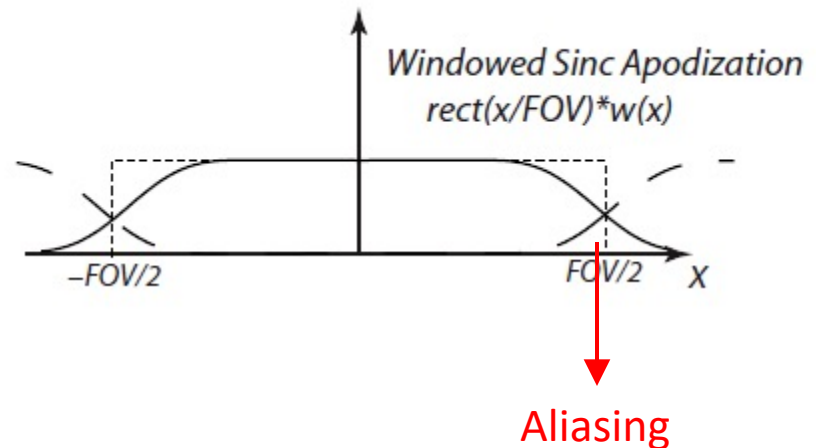
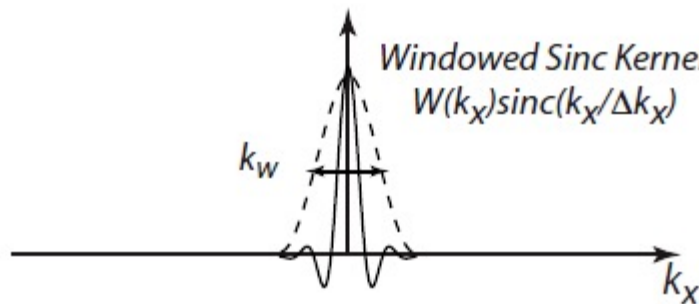


# Convolution kernel

- The ideal kernel would be an infinite sinc (impractical)



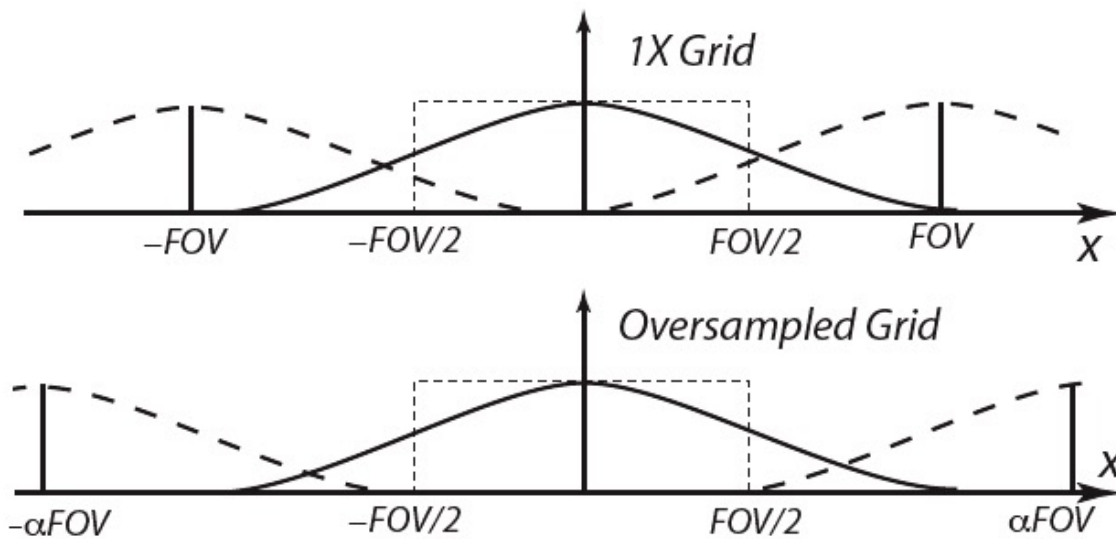
- Windowed sinc



# Oversampling the Cartesian grid

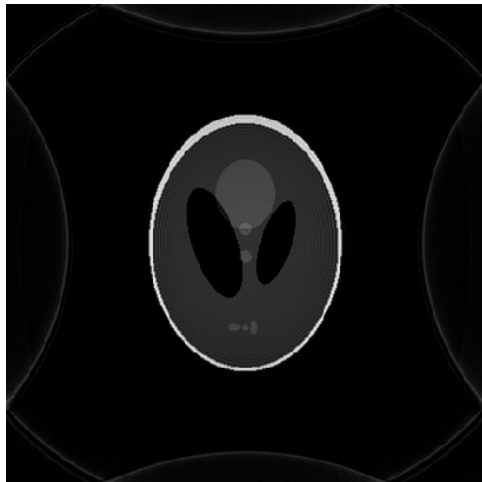
- Removes aliasing
- Reduces apodization

??

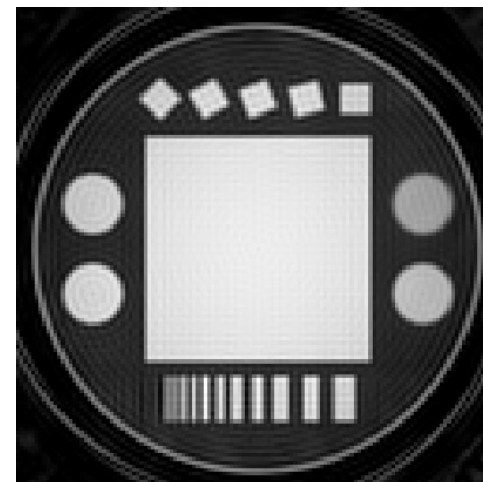
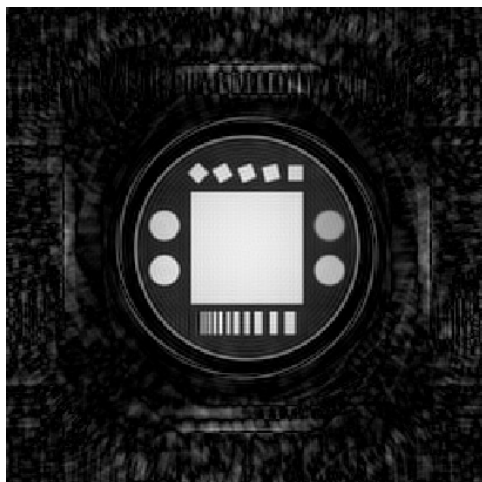
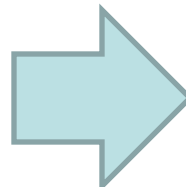


# Oversampling the Cartesian grid

2X grid



Crop in  
the image  
domain



# Convolution kernel

- Kaiser-Bessel function
  - Best kernel (by consensus)

$$C(k) = \frac{1}{W} I_0 \left( b \left( 1 - 2 \frac{k}{W} \right)^2 \right) \text{rect} \left( \frac{2k}{W} \right)$$

$I_0$ : zero-order modified Bessel function of the first kind

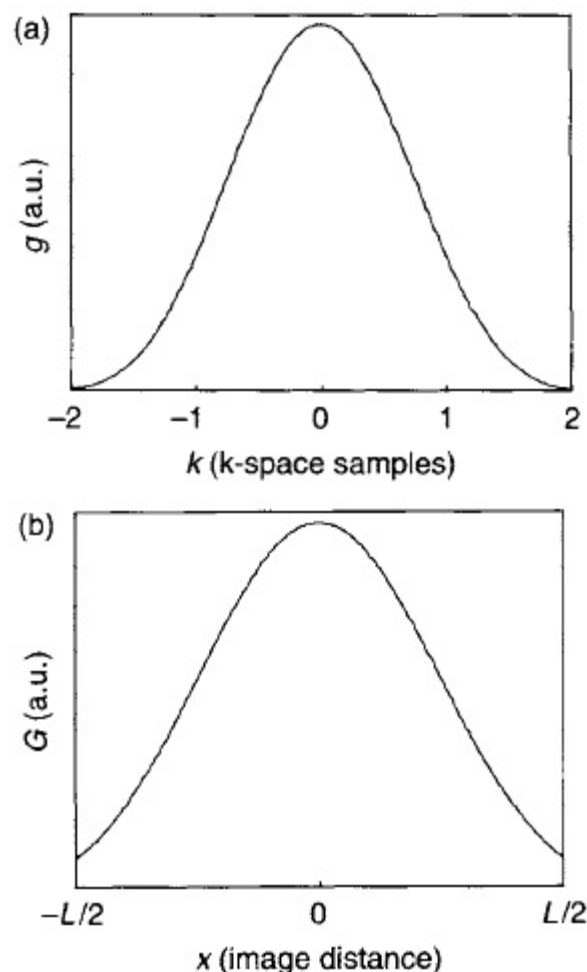
$W$ : width of the kernel

$b$ : scaling parameter

- Inverse Fourier transform

$$c(x) = \frac{\sin(\sqrt{\pi^2 W^2 x^2 - b^2})}{\sqrt{\pi^2 W^2 x^2 - b^2}}$$

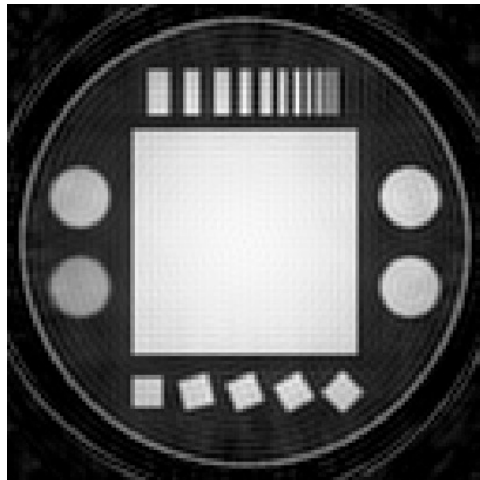
要是知道kernel的 inverse FFT,  
可以避免aliasing,因为可以直接使用  
kernel ifft的数学表达式, 得到MRI  
图片后再乘kernel的ifft表达式



# Why the Kaiser-Bessel kernel is preferred?

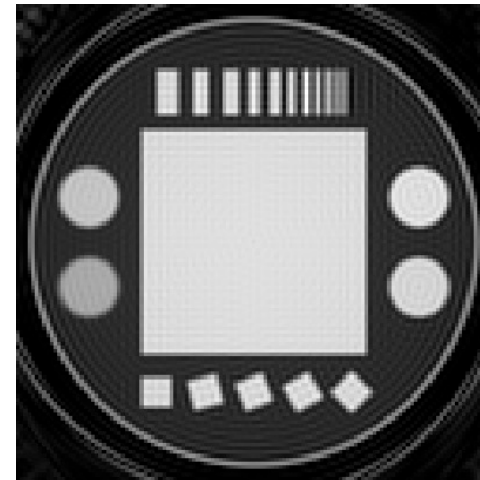
- Less oversampling

Triangular

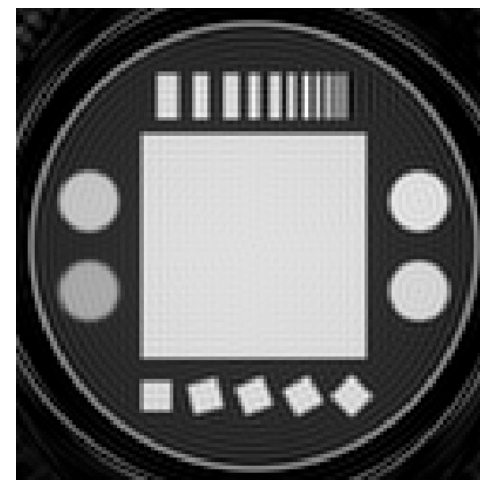
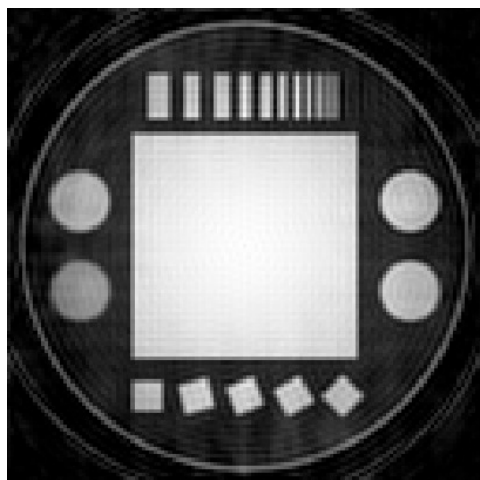


1.5X grid

Kaiser-Bessel

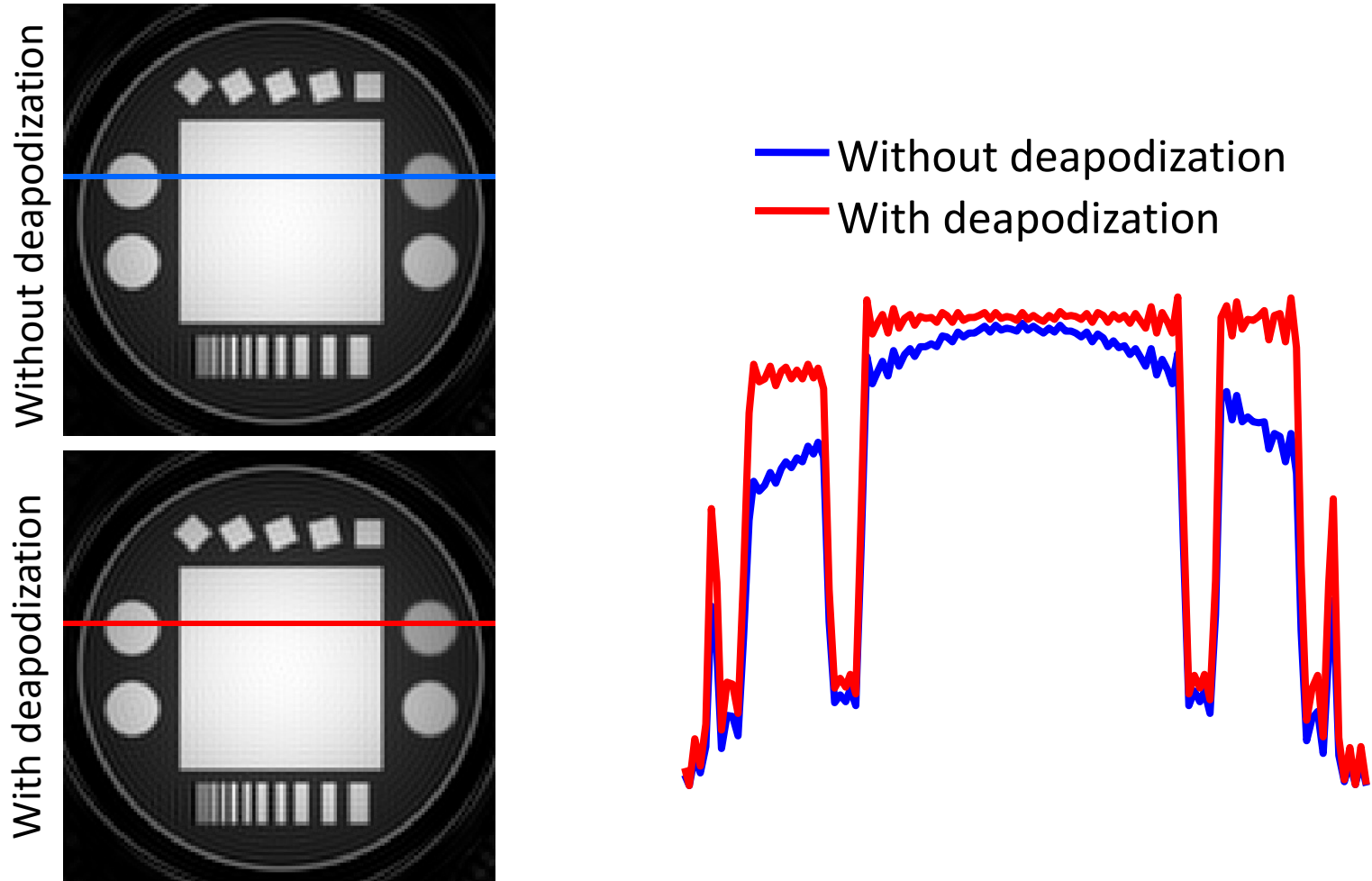


1.25X grid

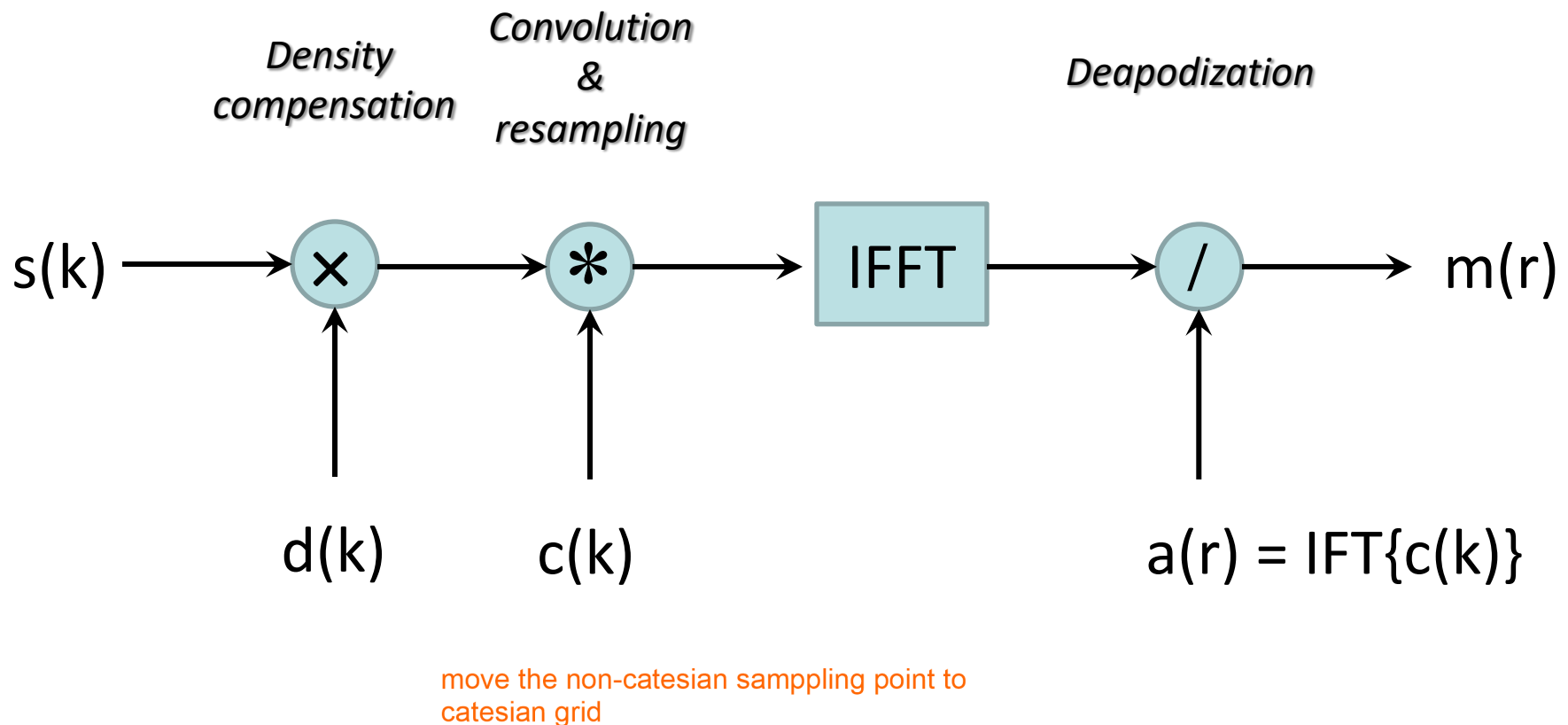


# Deapodization

- Divide the reconstructed image by the inverse Fourier transform of the gridding kernel



# Gridding reconstruction steps



# Summary of gridding reconstruction

- Compute the non-Cartesian k-space sampling pattern
- Choose the gridding kernel (e.g. Kaiser-Bessel)
  - map the non catesian to  
catesian grid
- Density pre-compensation (if possible)
- Convolve the pre-compensated k-space data with the gridding kernel and evaluate the convolution at the Cartesian grid (oversampled)
- Apply inverse FFT
- Apply deapodization function
- Remove the oversampling by cropping the image

# Non-Uniform FFT (NUFFT)

- Generalized version of the gridding algorithm
- Similar idea, but fast implementation
- Forward and adjoint operators
  - Very useful for iterative algorithms
- Popular implementation used by the MR community
  - J Fessler, University of Michigan

560

IEEE TRANSACTIONS ON SIGNAL PROCESSING, VOL. 51, NO. 2, FEBRUARY 2003

## Nonuniform Fast Fourier Transforms Using Min-Max Interpolation

Jeffrey A. Fessler, *Senior Member, IEEE*, and Bradley P. Sutton, *Member, IEEE*

*Abstract*—The fast Fourier transform (FFT) is used widely in signal processing for efficient computation of the FT of finite-length signals over a set of uniformly spaced frequency locations. However, in many applications, one requires nonuniform sampling in the frequency domain, i.e., a *nonuniform FT*. Several

argued compellingly for using trigonometric polynomials (complex exponentials) for finite-dimensional approximations in such problems [29] and proposed to use an iterative conjugate gradient reconstruction method with the nonuniform FFT (NUFFT) approach of [30] at its core. The min-max NUFFT

# Outlook exercise

## Computational MR imaging

### Laboratory 4: Reconstruction of non-Cartesian k-space data

Report is due on Wednesday the week after the lab session at 23:59. Send your report by email to Bruno Riemenschneider (bruno.riemenschneider@fau.de) and Florian Knoll (florian.knoll@fau.de).

#### Learning objectives

- Reconstruct non-Cartesian MRI data using gridding and NUFFT toolbox
- Apply gridding operations: density compensation, oversampling and deapodization
- Learn to use the NUFFT toolbox

1. **Radial sampling pattern:** Load radial\_data.mat (variable) and plot the acquired k-space. Each column corresponds to the readout dimension for each radial line. This data was acquired with a radial acquisition using a golden angle increment ( $111.246117975^\circ$ ). Generate a sampling trajectory that corresponds to this data for the reconstruction. **Figure 1** shows a plot of the first 10 spokes of such a trajectory for reference. If the matrix size for Cartesian imaging is 384x384, what is the number of radial lines corresponding to the Nyquist rate?

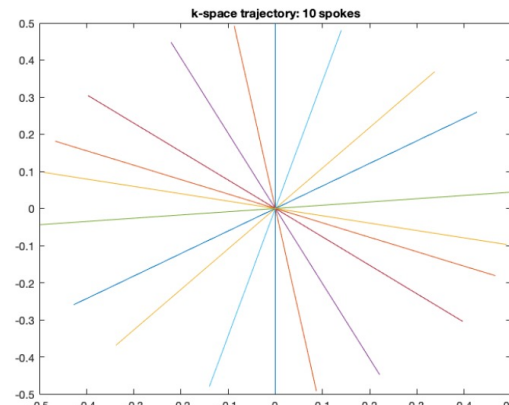


**Figure 1:** Radial trajectory with golden angle increment. Note that the first angle is at  $\pi/2$ .

2. **Basic gridding reconstruction:** Reconstruct this dataset using the provided grid1 function that grids 2D non-Cartesian k-space data to Cartesian k-space data using triangular gridding kernel of width 2:

Matlab version:  
function m = grid1(d,k,n)

% Input:

% d: non-Cartesian k-space data

% k: non-Cartesian k-space trajectory, each k(i) is a complex variable  
% where the real part is the kx coordinate and the imaginary part is the  
% ky coordinate.

% n: Cartesian grid size, e.g. [128x128]

% Output:

% m: gridded k-space data [nxn]

Python version:

def grid(d, k, n):

"""Grid non-cartesian kspace data to a cartesian grid

Keyword Arguments:

d - 2D numpy array, non-cartesian kspace

k - 2D numpy array, kspace trajectory, scaled -0.5 to 0.5

n - int, grid size

Returns:

2D numpy array (n, n)

Use a 384x384 Cartesian grid. Comment on the artifacts. Can you guess what organ was imaged?

3. **Density compensation:** Reconstruct the radial dataset from part 2 using a ramp filter. Plot your results. Do you need to employ oversampling and de-apodization on this dataset? Explain your answer.
4. **Oversampling:** Grid the decimated data from part 3 using oversampling factors of 1.5 and 2, apply inverse FFT and crop in the image domain.
5. **De-apodization:** Compute the de-apodization function in the image domain and apply to the gridded image with oversampling of 2.
6. **NUFFT toolbox:** Reconstruct the radial dataset using a widely used NUFFT toolbox from the research community. Plot your reconstructions and compare them with gridding reconstruction using the triangular kernel.
  - a. Matlab users: You will use the NUFFT toolbox from Jeffrey Fessler (University of Michigan). The toolbox is included as a zip file in the lab folder. You will have to include the folder in the Matlab path and then build a NUFFT object:  
$$\text{FT} = \text{NUFFT}(\text{data}, \text{density\_compensation}, 1, 0, \text{grid\_size}, 2);$$
This constructor initializes a NUFFT with a Kaiser-Bessel kernel.  
You can then access the forward and adjoint NUFFT by calling FT and FT'.
  - b. Python users: You will use the Torch KB-NUFFT toolbox from Matt Muckley (Facebook AI research). This toolbox is modeled after Jeffrey Fessler's toolbox. You can get it from github, and documentation is provided there:  
<https://github.com/mmuckley/torchkbnufft>